

Dark matter concentrations and a search for cores in Milky Way dwarf satellites

Joe Wolf & James S. Bullock

Center for Cosmology, Department of Physics and Astronomy, University of California, Irvine, CA 92697
wolfj@uci.edu, bullock@uci.edu

11 October 2018

ABSTRACT

We investigate the mass distributions within eight classical Milky Way dwarf spheroidal galaxies (MW dSphs) using an equilibrium Jeans analysis and we compare our results to the mass distributions predicted for subhalos in dissipationless Λ CDM simulations. In order to match the dark matter density concentrations predicted, the stars in these galaxies must have a fairly significant tangential velocity dispersion anisotropy ($\beta \simeq -1.5$). For the limiting case of an isotropic velocity dispersion ($\beta = 0$), the classical MW dSphs predominantly prefer to live in halos that are less concentrated than Λ CDM predictions. We also investigate whether the dSphs prefer to live in halos with constant density cores in the limit of isotropic velocity dispersion. Interestingly, even in this limit, not all of the dSphs prefer large constant-density cores: the Sculptor dSph prefers a cusp while Carina, Draco and Leo I prefer cores. The other four dSphs do not show a statistically significant preference for either cuspy or cored profiles. Finally, we re-examine the hypothesis that the density profiles of these eight MW dSphs can be quantified by a common dark matter halo.

Key words: Galactic dynamics, dwarf galaxies, dark matter

1 INTRODUCTION

The currently favored cold dark matter cosmology (Λ CDM) has had much success in reproducing the large scale structure of the universe (see Komatsu et al. 2011, and references therein). However, on smaller scales there are some possible discrepancies (e.g. Flores & Primack 1994; Moore 1994; Klypin et al. 1999; Moore et al. 1999; Boylan-Kolchin et al. 2011). One robust prediction from *dissipationless* Λ CDM simulations is that the inner density profile of dark matter halos should be fairly cuspy at small radii¹, with $\rho(r) \propto r^{-\gamma}$ and $\gamma \simeq 1$ (Dubinski & Carlberg 1991; Navarro et al. 1997; Diemand et al. 2008; Springel et al. 2008). In contrast, some observed rotation curves from dark matter dominated galaxies prefer fits with γ closer to 0 than 1 (e.g. de Blok et al. 2001; Simon et al. 2003, 2005; Kuzio de Naray et al. 2008; de Blok 2010). Even when fits to the rotation curves are forced to $\gamma = 1$ models, the resulting profiles are often less dense and less centrally-concentrated than predicted from dissipationless Λ CDM simulations (e.g., Alam et al. 2002).

At face value, the central density problem and cusp-core problem provides a challenge to cold dark matter theory.

Milky Way dwarf spheroidal galaxies (MW dSphs) provide particularly interesting dark matter laboratories. They include the most dark matter dominated systems known and are close enough to enable star-by-star kinematic studies (e.g. Walker et al. 2007; Simon & Geha 2007; Strigari et al. 2008; Geha et al. 2009; Lokas 2009; Kalirai et al. 2010; Martinez et al. 2011; Simon et al. 2011; Willman 2010; Willman et al. 2010; Wolf et al. 2010, hereafter W10). Unfortunately, because these objects are dispersion-supported their unknown stellar velocity anisotropy makes it difficult to determine their mass distributions using a simple projected Jeans analysis (e.g. Strigari et al. 2007a, W10).

In this paper, we ask whether a simple class of equilibrium models prefer solutions with dark matter densities that are consistent with Λ CDM expectations, and we also explore whether the solutions allow constant dark matter density in the inner parts, in conflict with naive expectations of Λ CDM theory.

Our work is motivated in part by the earlier study by Gilmore et al. (2007) (hereafter G07) where the results of an isotropic spherical Jeans analysis of the dispersion profiles of six of the eight brightest MW dSphs – Carina, Draco, Leo I,

¹ Interestingly, Peñarrubia et al. (2010) showed that dSphs are more likely to survive interactions with the MW disk if they are cusped rather than cored.

Leo II, Sextans, and Ursa Minor – were presented. The main result of G07 was that solutions to the Jeans equation for these systems prefer dark matter models with an “approximately constant density out to some break radius”. In this paper, we include all eight bright MW dSphs (excluding the tidally-disrupting Sagittarius dSph). Our results are different and do not lend support to the claim that all MW dSphs inhabit halos with large constant density cores. We look at the full probability distribution of the inner slope of the dark matter density profiles and find the spread in allowed values to be large enough that we cannot make a definitive statement for half of these dSphs. Among the other half, our analysis shows that Sculptor strongly prefers a cuspy halo.

We pay careful attention to the degeneracy of the dark matter density profile slope and the inner density profile of stars in our analysis. The inner density profile of the tracer stars (i.e. those with velocity measurements), as well as the stellar density profile derived from photometry, are uncertain in the inner parts. This uncertainty introduces significant uncertainty in the determination of the dark matter density profile – a point highlighted recently in Strigari et al. (2010) (hereafter S10). We note that this degeneracy is significant, even in comparison to the well-known degeneracy of the mass profile with the unknown velocity dispersion anisotropy.

Our conclusions are conservative in the sense that we force the inner light profiles to follow King (1962) models, which tend to bend sharply to cored light distributions as $r \rightarrow 0$ and thus favor more core-like mass densities (see §2). King profiles are not unique fits for these systems, and by allowing a broader range of stellar profile shapes a wider range of density profile slopes become possible (S10).

If there are constant density cores at the centers of small dark matter halos it could signal the existence of non-standard dark matter particles (e.g. Hogan & Dalcanton 2000; Avila-Reese et al. 2001; Kaplinghat 2005; Strigari et al. 2007c). A modified dark matter solution would be particularly attractive if these cores were ubiquitous and of approximately the same density. Density cores might alternatively arise from baryonic physics that alters the dark matter distributions compared to dissipationless simulations (as demonstrated explicitly by Mashchenko et al. 2008; Governato et al. 2010; Pasetto et al. 2010; Oh et al. 2011). The feedback processes that give rise to such cores rely on potentially stochastic details like the fraction of baryons that have been converted into stars (e.g. Brook et al. 2011). Therefore, if the cores are created by feedback processes, one might expect that the central density structure of dark matter halos will demonstrate significant variations from halo to halo, as seems to be the case for low surface brightness galaxies (Kuzio de Naray et al. 2010).

Lastly, we further explore the anisotropy-slope degeneracy in order to address the question of what anisotropies are needed in order for simulations to reproduce these MW dSphs, if they are to live in Λ CDM-like halos.

In the next section we provide a discussion of the degeneracies inherent in the use of Jeans modeling to constrain density profile slopes, even under the assumption of isotropy. We present our analysis and results in §3, where we discuss the mass modeling for each dSph, the question of a common halo for all the dSphs, the most probable stellar velocity

dispersion anisotropies required to fit NFW profiles to the dSphs and a comparison of concentrations to those seen in recent Λ CDM simulations. We also discuss both the requirements for our cuspy density profile fits to be physical when isotropy is assumed and the complexities in the stellar population that we do not take into account in this work. We summarize our results in §4.

2 EXPECTATIONS FROM THE JEANS EQUATION

The spherical Jeans Equation relates the integrated mass of a spherically symmetric, dispersion-supported, collisionless system to its tracer velocity dispersion and tracer number density $n_*(r)$, under the assumption of dynamical equilibrium:

$$M(r) = \frac{r \sigma_r^2}{G} (\gamma_* + \gamma_\sigma - 2\beta). \quad (1)$$

Here $\sigma_r(r)$ is the radial velocity dispersion of the tracers and $\beta(r) \equiv 1 - \sigma_t^2/\sigma_r^2$ quantifies the tangential velocity dispersion. The additional terms quantify radial gradients in the stellar distribution $\gamma_* \equiv -d \ln n_*/d \ln r$ and velocity dispersion profile $\gamma_\sigma \equiv -d \ln \sigma_r^2/d \ln r$. While β , and to a lesser extent γ_σ , are difficult to determine empirically, γ_* is in principle constrained by observations. If we assume a form of the anisotropy then γ_σ can be solved for directly (see Mamon & Boué 2010, and Equations A7-9 in W10), and thus the Jeans equation immediately provides a path towards direct mass constraints. If we further assume that the stellar system is isotropic ($\beta = 0$), then our analysis simplifies considerably.

However, even with the assumption of isotropy, constraints on the slope of the mass density profile $\gamma \equiv -d \ln \rho/d \ln r$ will require knowledge of the second derivatives of both $n_*(r)$ and $\sigma_r(r)$, which will necessitate exquisite data sets. Typically, $n_*(r)$ is assumed to follow an empirically-motivated functional form, without significant concern for the allowed freedom of its detailed curvature at small radius. For purposes of comparison, we will follow G07 and assume that $n_*(r)$ tracks a King (1962) profile. As we will now demonstrate, this is conservative in the sense that it forces a sharply flattening inner slope for the tracer stars, which in turn favors a flatter density slope γ at small r than might otherwise be allowed. Indeed, S10 found that most of the available photometric data for the classical dSphs can be fit with divergent 3D number densities that asymptote slowly to power-laws. In this sense, the inner density slopes derived in this paper are biased to favor more core-like behavior.

One can understand how the shape of $n_*(r)$ affects core vs. cusp determinations by considering a proxy for the density profile slope $\gamma \simeq \aleph \equiv 3 - d \ln M/d \ln r$. For $\beta = 0$, Equation 1 implies $\aleph = 2 + \gamma_\sigma - (\gamma'_* + \gamma'_\sigma)/(\gamma_* + \gamma_\sigma)$, where the primes indicate derivatives with respect to $\ln r$. If we define

$$\kappa_* \equiv \gamma'_*/\gamma_* \quad (2)$$

in order to quantify the curvature of the light profile, we can rewrite the density slope proxy as

$$\aleph = 2 + \gamma_\sigma - \gamma'_\sigma (\gamma_* + \gamma_\sigma)^{-1} - \kappa_* (1 + \gamma_\sigma/\gamma_*)^{-1}. \quad (3)$$

Table 1: Derived parameters of MW dSphs when modeled under the assumption of isotropy.

Galaxy	$r_{1/2}$ [pc]	C_{King}	$\kappa_*(r_{1/2})$	$\gamma(r \rightarrow 0 \text{ pc})$	$\gamma(100 \text{ pc})$	$\gamma(r_{1/2})$	$\log_{10}(\rho_{\text{core}} r_{\text{core}} M_{\odot}^{-1} \text{pc}^2)$	r_{core} [pc]
Carina	334	3.3	1.9	$0.0^{+0.5}_{-0.2}$	$0.4^{+0.3}_{-0.2}$	$0.4^{+0.4}_{-0.3}$	$1.2^{+1.2}_{-0.1}$	—
Draco	291	5.9	1.2	$0.0^{+0.4}_{-0.2}$	$0.3^{+0.3}_{-0.2}$	$0.5^{+0.3}_{-0.1}$	$2.0^{+0.4}_{-0.3}$	—
Fornax	944	5.2	0.8	$0.7^{+0.3}_{-0.4}$	$0.8^{+0.2}_{-0.2}$	$1.4^{+0.3}_{-0.1}$	$1.1^{+0.04}_{-0.03}$	790^{+130}_{-110}
Leo I	388	1.9	2.7	$0.0^{+0.4}_{-0.1}$	$0.2^{+0.3}_{-0.1}$	$0.4^{+0.4}_{-0.2}$	$2.3^{+0.5}_{-0.6}$	—
Leo II	233	3.5	2.2	$0.5^{+0.6}_{-0.3}$	$0.8^{+0.5}_{-0.4}$	$1.2^{+1.6}_{-0.5}$	$1.4^{+1.7}_{-0.1}$	—
Sculptor	375	13	0.5	$1.1^{+0.1}_{-0.5}$	$1.2^{+0.1}_{-0.4}$	$1.3^{+0.2}_{-0.1}$	$0.61^{+0.27}_{-0.04}$	410^{+80}_{-70}
Sextans	1019	9.6	2.4	$0.7^{+0.4}_{-0.4}$	$0.8^{+0.4}_{-0.3}$	$1.5^{+0.5}_{-0.3}$	$0.61^{+0.27}_{-0.15}$	660^{+280}_{-200}
Ursa Minor	588	4.4	1.1	$0.3^{+0.6}_{-0.2}$	$0.5^{+0.4}_{-0.3}$	$1.0^{+0.5}_{-0.4}$	$1.5^{+0.7}_{-0.1}$	—

Note: Mean values of deprojected half-light radii ($r_{1/2}$) are from Table 1 of W10 while the mean King concentrations $C_{\text{King}} \equiv (r_{\text{lim}}/r_{\text{King}})$ and κ_* values are derived from the photometric properties listed in Table 1 of W10. Here $\kappa_*(r_{1/2})$ quantifies the curvature of the light profile at $r_{1/2}$, as defined by Equation 2. As discussed in the text, galaxies whose light profiles have smaller values of the curvature will tend to favor cuspy overall density profiles. The total density log-slopes $\gamma(r) = -d \ln \rho / d \ln r$ in the next three columns are derived when utilizing Equation 4. The density parameters in the last two columns are derived by utilizing the Burkert profile (Equation 5). Errors correspond to 68% likelihood values.

At radii near the the deprojected half-light radius $r \simeq r_{1/2}$, the term multiplying κ_* in Equation 3 is positive and of order unity², which implies that a larger κ_* will favor a smaller \aleph and a more core-like distribution. In the limit where γ_{σ} and γ'_{σ} are small, κ_* will dictate the inferred density slope.

To illustrate this point, consider the light profile of the Carina dSph, which prefers the parameter combination $r_{\text{lim}}/r_{\text{King}} = 3.27$ with a deprojected half-light radius $r_{1/2} = 334$ pc when fit with a King profile (see Table 1 of W10). S10 showed that the same photometry can be fit by a stellar light profile that is divergent at the center (with approximately the same half-light radius). At $r \simeq r_{1/2}$ both the S10 fit and the King fit have similar curvature: $\kappa_*(r_{1/2}) = 1.05$ and 1.12 , respectively. But at the slightly smaller radius $r = 0.5 r_{1/2}$ the light profile favored by S10 has a significantly smaller curvature $\kappa_* = 1.5$ compared to the King fit $\kappa_* = 2.4$, and this difference further increases at smaller radii, where κ_* diverges at small r for the King profile but drops to zero for the S10 fit. Indeed, compared to other common light distributions, the King fit imposes the strongest curvature towards small r and this will act to push solutions towards more core-like mass density profiles. For example, a Plummer (1911) profile has $\kappa_*(0.5 r_{1/2}) = 1.4$ and a Hernquist (1990) profile has $\kappa_*(0.5 r_{1/2}) = 0.3$. Thus, for a fixed σ_r , King profiles will prefer smaller overall density profile slopes than all of the common alternatives.

The above discussion highlights the difficulties associated with accurately constraining central density profile slopes using Jeans analysis. A similar point was emphasized by S10. In practice, one would need to know κ_* and γ'_{σ} very accurately at small radii in order to definitively constrain the asymptotic density profile slope, even with the assumption of isotropy. Our approach instead is to adopt a conservative (and standard) assumption of the King tracer distribution, which will allow us to directly compare with the work of G07. We show that even in this limit, not all of the dSph galaxies prefer core-like distributions.

² This is because most commonly-used stellar tracer distributions yield $\gamma_* \simeq 3$ at $r_{1/2}$ (see Appendix B of W10) and empirically we expect $|\gamma_{\sigma}| < 1$ owing to the rather flat velocity dispersion profiles observed (see Equations A7-9 of W10).

3 DYNAMICAL ANALYSIS

We use a spherical Jeans analyses to constrain the density profile slopes of the eight classical MW dSphs: Carina, Draco, Fornax, Leo I, Leo II, Sculptor, Sextans, and Ursa Minor. The kinematic and photometric data we use are referenced in Figure 2 and Table 1 of W10 (Muñoz et al. 2005; Koch et al. 2007; Mateo et al. 2008; Walker et al. 2009a). We constrain the allowed mass profile for each dwarf using a Bayesian analysis as described in Martinez et al. (2009) and W10.

We marginalize over a generalized density profile described by six parameters

$$\rho_{\text{tot}}(r) = \frac{\rho_s e^{-r/r_{\text{cut}}}}{(r/r_s)^c [1 + (r/r_s)^a]^{(b-c)/a}}, \quad (4)$$

using the same prior ranges discussed in Section 2.3 of W10. When noted, we have also considered the Burkert (1995) profile

$$\rho_{\text{tot}}(r) = \frac{\rho_{\text{core}}}{(1 + r/r_{\text{core}})(1 + (r/r_{\text{core}})^2)} \quad (5)$$

for comparison, with the same above priors for the scale radii and densities. In all of our analyses we marginalize over the photometric uncertainties of the fitted King (1962) profiles (see Table 1 of W10). Finally, unless otherwise stated, we force the velocity dispersion tensor to be isotropic ($\beta = 0$).

3.1 Density profiles for individual dSphs

Table 1 summarizes results from our isotropic Jeans analysis for each of the eight galaxies we consider. The first three columns list relevant observational parameters, while the middle three columns list the derived constraint on the local density profile slope at three example radii: an asymptotic inner radius ($r \rightarrow 0$ pc), an intermediate radius (100 pc), and at $r_{1/2}$. The last two columns display results from our analysis of constraining the density profile by Equation 5. As is shown in the table, and as is highlighted in our discussions below, some of the galaxies prefer cusps, some prefer cores, and others are indeterminate. Also, as expected from the discussion above, galaxies with the smallest curvature in their light profiles κ_* (column 3) tend to be those that prefer the most cuspy overall density profiles ($\gamma \sim 1$).

Posterior distributions for the asymptotic inner slope

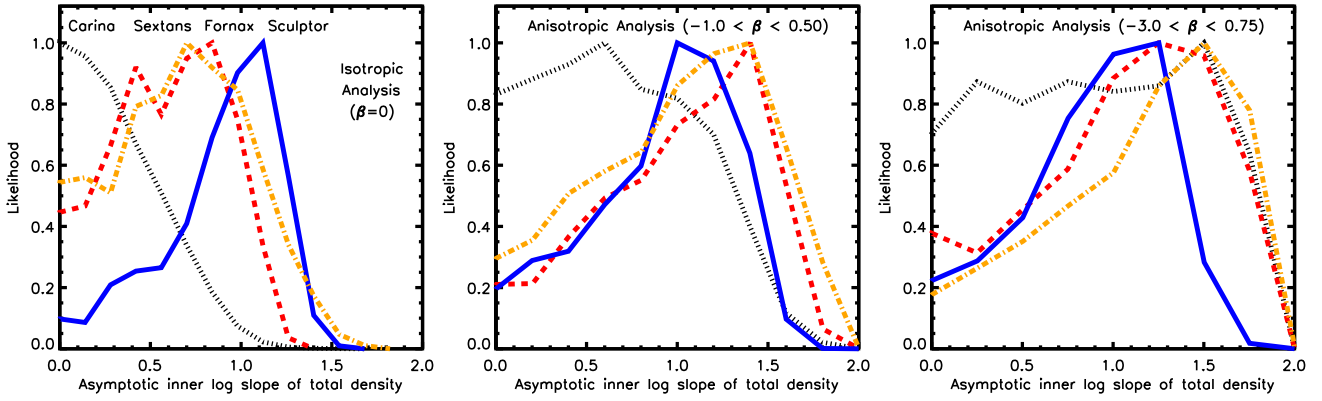


Figure 1. Probability densities for $\gamma(r) = -d \ln \rho / d \ln r$ as $r \rightarrow 0$ when modeling with Equation 4 the four MW dSphs with the highest quality kinematic data which is publicly available: Carina (black dotted), Fornax (red dashed), Sculptor (blue solid), and Sextans (orange dot-dashed). (a): Isotropic analysis ($\beta = 0$). This result shows that not all of the classical MW dSphs prefer to be cored ($\gamma \simeq 0$) under the assumption that $\beta = 0$. (b) and (c): Anisotropic analyses demonstrating how the likelihood for γ widens as the range on the allowed anisotropies widens.

are presented in Figure 1 for the four dSphs that contain the largest published kinematic datasets (Walker et al. 2009a). The left panel shows slope distributions for our isotropic analysis. Carina (black dotted) demonstrates a strong preference for living in a cored dark matter halo ($\gamma \simeq 0$), while Fornax (red dashed) and Sextans (orange dot-dashed) prefer moderate cusps ($\gamma \simeq 0.7$), but their distributions are too wide to draw any strong conclusions.

The most interesting case is Sculptor (solid blue), which shows a strong preference for living in a cuspy dark matter halo with $\gamma \simeq 1$. Sculptor’s line-of-sight velocity dispersion profile rises more rapidly in its center than any of the other well-studied MW dSphs, which drives the data to prefer cuspy profiles when isotropy is assumed. The physical reasoning for this is discussed in Section 3.1 of W10. Briefly, as one observes closer to the center of a system, the intrinsic radial dispersion projects onto the line-of-sight dispersion. Thus, a sharp rise in the observed dispersion could only be produced by two effects: the presence of a rising density (i.e. a cusp) or a highly radial stellar anisotropy. Since we are assuming isotropy in our analysis, a cusp naturally arises.

The middle and right panels of Figure 1 show how the asymptotic density slope distributions widen as we allow for wider ranges of (constant) velocity dispersion anisotropy, $-1.0 < \beta < 0.5$ and $-3.0 < \beta < 0.75$. Though not shown here, we also explored a case where the concentrated stellar component of Fornax was included in the total mass profile with a constant V-band mass-to-light ratio of $\Upsilon = 2$. Despite the relatively low dynamical mass-to-light ratio of this galaxy ($\Upsilon_{1/2}^V \simeq 9$; see Table 1 of W10) we did not find any statistically significant change in the inner dark matter slope distribution.

Figure 1 shows that under the assumption of isotropy at least one MW dSph (Sculptor) strongly prefers being hosted in a cuspy dark matter halo.³ Inspection of Table 1 further reveals that four of the eight classical dSphs are consistent (one sigma) with inner cusps of $\gamma = 1$, while three of the eight dSphs prefer asymptotic slopes of $\gamma \simeq 0$ at one sigma.

We also ran an alternate analysis where we set the mass

density to be a Burkert profile (Equation 5) along the lines of the analysis in Donato et al. (2009) (hereafter D09) where it was proposed that over a wide range of luminosities, galaxies (including the six dSphs in G07) can be fit by cored Burkert profiles that have core densities and core radii related via $\rho_{\text{core}} \propto r_{\text{core}}^{-1}$ such that $\rho_{\text{core}} r_{\text{core}} = 10^{2.15 \pm 0.2} \text{ M}_{\odot} \text{ pc}^{-2}$, independent of luminosity. Our results (see Table 1) show about a factor of four spread in the mean $\log_{10}(\rho_{\text{core}} r_{\text{core}})$ values with the actual values for $\log_{10}(\rho_{\text{core}} r_{\text{core}})$ about a factor of two smaller than those in D09. While the product of $\rho_{\text{core}} r_{\text{core}}$ is always well constrained, only three dSphs (Fornax, Sculptor, and Sextans) have constraining posterior distributions for r_{core} .

Before moving on, we point out that each of these three galaxies have $r_{\text{core}} \simeq r_{1/2}$. Given that $\gamma(r_{\text{core}}) = 1.5$ for a Burkert profile, these results do not indicate disagreement with dissipationless Λ CDM simulations, which show that dark matter halos have similar values for γ around the same physical radii.

3.2 Global population of MW dSphs

We now move on to Figure 2, where the points presented in the left panel show the average density of each dSph within its deprojected half-light radius $\langle \rho \rangle_{1/2}$ as a function of $r_{1/2}$. Our motivation for examining the density within $r_{1/2}$ is that constraints on the mass density within the *deprojected* half-light radius are less sensitive to assumptions about the velocity dispersion anisotropy, and thus they are more directly constrained by data (W10). The right panel of Figure 2 shows the derived local log-slope at $r_{1/2}$ as a function of $r_{1/2}$ for the same set of galaxies under the assumption of isotropy.

Recently, there have been several papers pointing out that the MW dSphs are consistent with inhabiting similar cuspy dark matter halos (Strigari et al. 2008; Walker et al. 2009b, W10).⁴ Additionally, the mass within $r_{1/2}$ has been

³ Note that G07 did not analyze Fornax or Sculptor.

⁴ Note that Mateo et al. (1993) suggested that the classical dSphs had similar masses within their stellar extent. However,

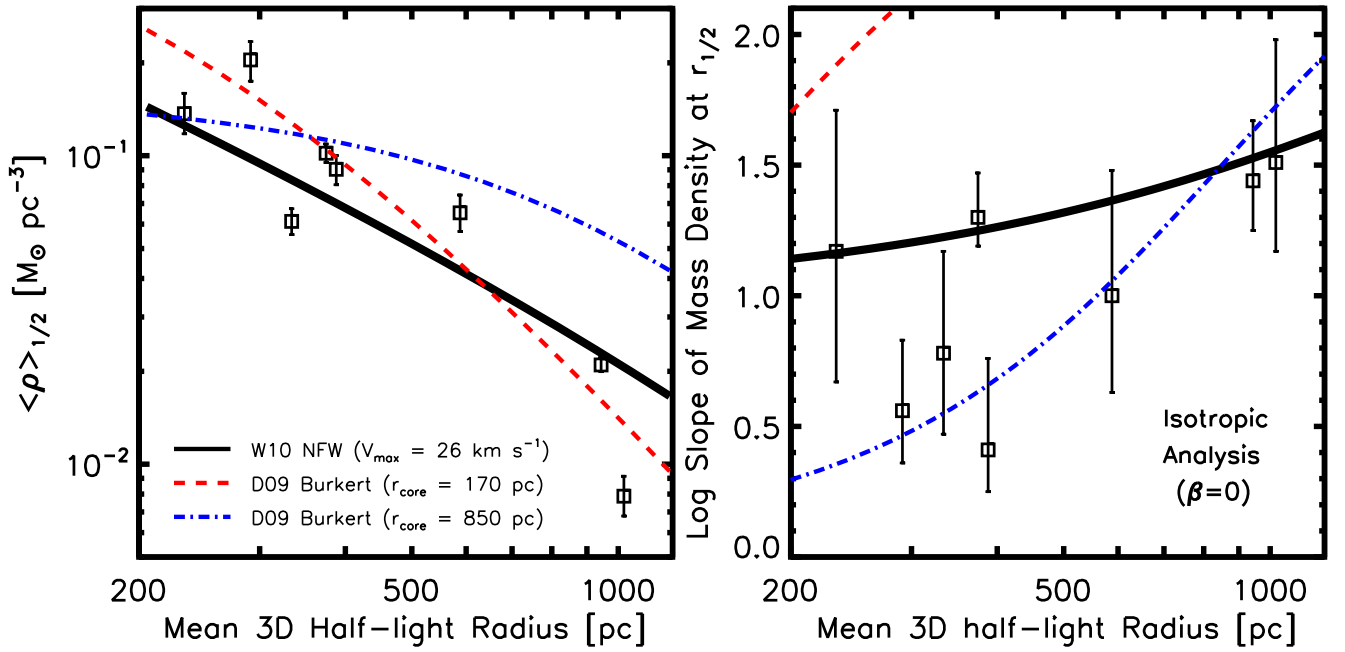


Figure 2. Can a common halo reproduce all of the data? The solid black lines in each panel show the implied trends for a typical *field* NFW halo with maximum circular velocity $V_{\text{max}} = 26 \text{ km s}^{-1}$ with $r_{\text{max}} = 5.7 \text{ kpc}$ (the same NFW halo presented in Figure 3 of W10). We note that this is less dense than a typical subhalo of the same V_{max} in recent dark-matter-only simulations of halos similar to the Milky Way. The two colored lines show cored Burkert profiles that obey the D09 constant surface density constraint with core radii of 170 pc (red dashed) and 850 pc (blue dot-dashed). Of these two, only the small cored halo provides a reasonable characterization of all the data in the left panel, but the same halo fails to reproduce the log-slope information in the right panel for any of the data. Meanwhile, the large cored halo only fares well at describing some of the data in the right panel. Of the three plotted, the cuspy NFW halo fares best at describing the full population within a common halo. However it is only consistent at the $2 - \sigma$ level with predictions of the $r_{\text{max}} - V_{\text{max}}$ relation from recent simulations.

shown to increase roughly as $M_{1/2} \sim r_{1/2}^2$ (Tollerud et al. 2011; Walker et al. 2010, W10), which is what one would expect if all of the galaxies were embedded within similar dark matter halos that each obeyed the density scaling $\rho(r) \sim r^{-1}$. This is illustrated in the left panel of Figure 2, where the solid black line shows a NFW density profile (which scales as r^{-1} at small r ; see Navarro et al. 1997) for a halo of virial mass $3 \times 10^9 M_{\odot}$ and a typical concentration for a *field* halo (the same halo shown in Figure 3 of W10, which was chosen to represent all of the MW dSphs, not just the classical MW dSphs).

To more accurately assess the hypothesis that all of the MW dSphs lie in similar dark matter halos, one needs to simultaneously examine both the density *and* the log-slope of the population. We begin by noting the colored lines in Figure 2, which show the implied $\langle \rho \rangle(< r)$ vs. r and $\gamma(r)$ vs. r relations for two example cored Burkert profiles – one with a small core (red dashed with $r_{\text{core}} = 170 \text{ pc}$) and another with a large core (blue dot-dashed with $r_{\text{core}} = 850 \text{ pc}$). The core densities for each of the Burkert profiles were chosen to follow the previously mentioned trend advocated by D09.

As can be seen in the left panel of Figure 2, in order to match the density vs. radius relation for the sample of dSphs we need a Burkert profile that has a core radius that is smaller than the smallest half-light radius in our sam-

ple $r_{\text{core}} \lesssim 200 \text{ pc}$. Although this point was mentioned by Walker et al. (2009b), if we were to include the ultrafaint MW dSphs as they did, the core size would need to be approximately the size of Segue 1 ($r_{1/2} \simeq 40 \text{ pc}$; see Table 1 of W10) in order to provide a decent fit to the data. Moreover, the same small-core Burkert that best fits the data in the left panel does poorly in the right panel because it is *too steep* to characterize the population. The large-core Burkert profile (blue dot-dashed) does better at fitting the data in the right panel but does much worse in the left panel because the implied core is *too large*. Overall, while it is possible to fit each individual dSph galaxy with a Burkert profile obeying a scaling of $\rho_{\text{core}} \propto r_{\text{core}}^{-1}$ (see Table 1), it is not possible to find a common cored halo solution that adequately reproduces the population (i.e. choosing Burkert profiles with intermediate core sizes fail in both plots).

However, although it is certainly not a perfect fit to all of the data points in the right panel, the W10 NFW halo has a local log-slope profile that is consistent at one sigma with five of the eight dSphs while also faring well in the left panel (interestingly, six of the eight galaxies are one sigma consistent with a log-slope at $r_{1/2}$ steeper than $\gamma = 1$). Also note that a NFW halo with a scale radius smaller than a kpc (like the one advocated for by Walker et al. 2009b) will not provide a good fit to the data in the right panel of Figure 2.

It should be pointed out, however, that the NFW profile plotted in this figure is lower than the median predictions from the Aquarius and Via Lactea 2 simulations. Thus, Figure 2 makes it clear that $\beta = 0$ is not a good assumption

the mass estimator used was not accurate (see Appendix C of W10 for an explanation), and thus the claim is not true.

when attempting to place MW dSphs in cuspy dark matter halos. We discuss this further in Section 3.5.

3.3 Are the solutions physical?

The solutions obtained by imposing the Jeans equation are not guaranteed to have a positive definite distribution function. Here we investigate how a cuspy dark matter density profile is consistent with $\beta = 0$ and $\gamma_*(r \rightarrow 0) \rightarrow 0$. Previous work by An & Evans (2006) [also see White (1981) and de Bruijne et al. (1996) for scale-free potential and stellar profiles] has shown that the log-slope of the external potential should satisfy an inequality in order for the distribution function to be positive definite. The results in An & Evans (2006) were noted in the limit $r \rightarrow 0$, but are applicable everywhere. Here we briefly recall their arguments.

We assume, as in An & Evans (2006), that the distribution function of the stars has the form $f(E, L) = L^{-2\beta} g(E)$ and that the dark matter provides an external potential for this stellar system such that the mass profile is monotonically decreasing with radius. Given the assumption of a constant β ,

$$n_*(r) \propto r^{-2\beta} (-\phi(r))^{1/2-\beta} \int_{\phi}^0 (1 - E/\phi(r))^{1/2-\beta} g(E) dE, \quad (6)$$

where $\phi(r)$ is the gravitational potential sourced by the dark matter density profile, and the constant of proportionality is a positive definite function of β . We neglect the influence of stars on the gravitational potential, which is a good approximation for the dSphs. With this, it is simple to show that $k(r) = n_*(r)r^{2\beta}(-\phi(r))^{\beta-1/2}$ is a monotonically decreasing function of ϕ for $\beta < 1/2$. Since $d\phi(r)/dr > 0$ and $k(r) > 0$, we have $d \ln k(r)/d \ln r \leq 0$. This constraint implies:

$$\gamma_*(r) \geq 2\beta + (1/2 - \beta)\delta(r), \quad (7)$$

where $-\delta(r) = d \ln(-\phi(r))/d \ln r > 0$ is the log-slope of the external (i.e. dark matter) gravitational potential. For $\beta = 0$, we have $\delta(r) \leq 2\gamma_*(r)$. For dark matter density profiles that diverge more slowly than $1/r^2$ as $r \rightarrow 0$, we have $\delta(r) \rightarrow 0$. However, this is not sufficient since we have also assumed that $\gamma_*(r) \rightarrow 0$ as $r \rightarrow 0$.

The log-slope of the potential may be written as:

$$\begin{aligned} \delta(r) &= \frac{V_c^2(r)}{V_c^2(r) + 4\pi G \int_r^\infty \rho(x)x dx} \\ &\simeq \frac{V_c^2(r)}{4.5V_{\max}^2} \simeq 0.5(r/r_s)^{2-\mathfrak{I}} \quad \text{as } r \rightarrow 0 \end{aligned} \quad (8)$$

where $V_c(r)$ is the circular velocity and V_{\max} is the maximum circular velocity. To derive the final approximation on the second line we have assumed that the dark matter density profile diverges as $(r/r_s)^{-\mathfrak{I}}$ for $r \ll r_s$. The constants in the approximations in the second line are a fit for a NFW profile but work well for all commonly used cored and cuspy dark matter halo density profiles. Since $\gamma_*(r) \propto (r/r_{\text{King}})^2$ as $r \ll r_{\text{King}}$, we see that the constraint $\delta(r) < 2\gamma_*(r)$ will be violated at small radii because $2\gamma_*$ for our tracer density (a King profile) asymptotes to 0 more quickly than δ as $r \rightarrow 0$.

We may estimate the radius at which this constraint is violated by noting that $\gamma_*(r) \simeq 3(r/r_{\text{King}})^2$ for typically observed values of the concentration of MW dSphs, and hence $\delta(r) > 2\gamma_*(r)$ for $r \lesssim r_s(0.3r_{\text{King}}/r_s)^{2/\mathfrak{I}}$. For typical values,

such as $\mathfrak{I} = 1$, $r_{\text{King}} = 0.3 \text{ kpc}$, $r_s = 1 \text{ kpc}$, the constraint is violated at radii smaller than about 10 pc.

Given that both photometric and kinematic data of MW dSphs are scarce in the region $r \lesssim 10 \text{ pc}$ (often the errors on the position of the center of the MW dSphs are larger than this), substitution of a dark matter distribution with a small core or a profile that becomes more shallow with decreasing radius (such as the profile presented in Einasto 1965) would have little effect on our results outside of this region. In fact, recent high-resolution Λ CDM simulations do not lend support to the expectation that the inner density profile log-slope converges to -1, as an Einasto profile with a gradually decreasing log-slope amplitude seems to be a better fit (e.g. Springel et al. 2008; Diemand et al. 2008). Thus, the implications of our isotropic results would not change were we to fulfill the requirements of a positive definite distribution function.

3.4 Multiple stellar populations

Our analysis assumes that the entire spectroscopic sample follows a spatial distribution that is well described by the adopted photometric surface brightness fits. We have allowed for errors in the surface brightness fits, but not for the possibility that there are multiple populations with distinct velocity dispersions.

The motivation to model systems with multiple tracer components can be understood from the main analytic result of W10, which shows that the mass within a radius near the deprojected half-right radius can be determined nearly independent of stellar velocity dispersion anisotropy. If two subpopulations have different half-light radii, then one knows the mass well at two different locations, and thus the effects of the mass-anisotropy degeneracy are substantially reduced. This technique was first attempted by Battaglia et al. (2008, hereafter B08) who modeled the Sculptor dSph assuming separate metal-rich and metal-poor stellar populations. In their analysis, B08 found that Sculptor prefers a cored mass distribution.⁵

The newer publicly available dataset for Sculptor (Walker et al. 2007, 2009a,c) that we use contains approximately three times more velocity measurements than in the B08 sample, and many new spectra are closer to the projected center. We emphasize that this larger data set has not been used to study the issue of multiple populations. Further, B08 impose a strict prior of radial anisotropy (that increases with distance from the center) in their modeling and this could also skew the results in favor of cored profiles (see Section 3.5).

The most important aspects to address when including information from multiple tracer populations in dynamical modeling include both deciding to which population each star (for which we have a velocity measurement) belongs and correctly modeling the underlying radial distributions of the subpopulations. For example, in B08 the two subpopulations are identified in the spectroscopic sample based on a sharp

⁵ While this work was being prepared for publication we became aware of the paper by Amorisco & Evans (2012), which used the B08 data to perform a similar analysis. Our comments regarding B08 apply also to this work.

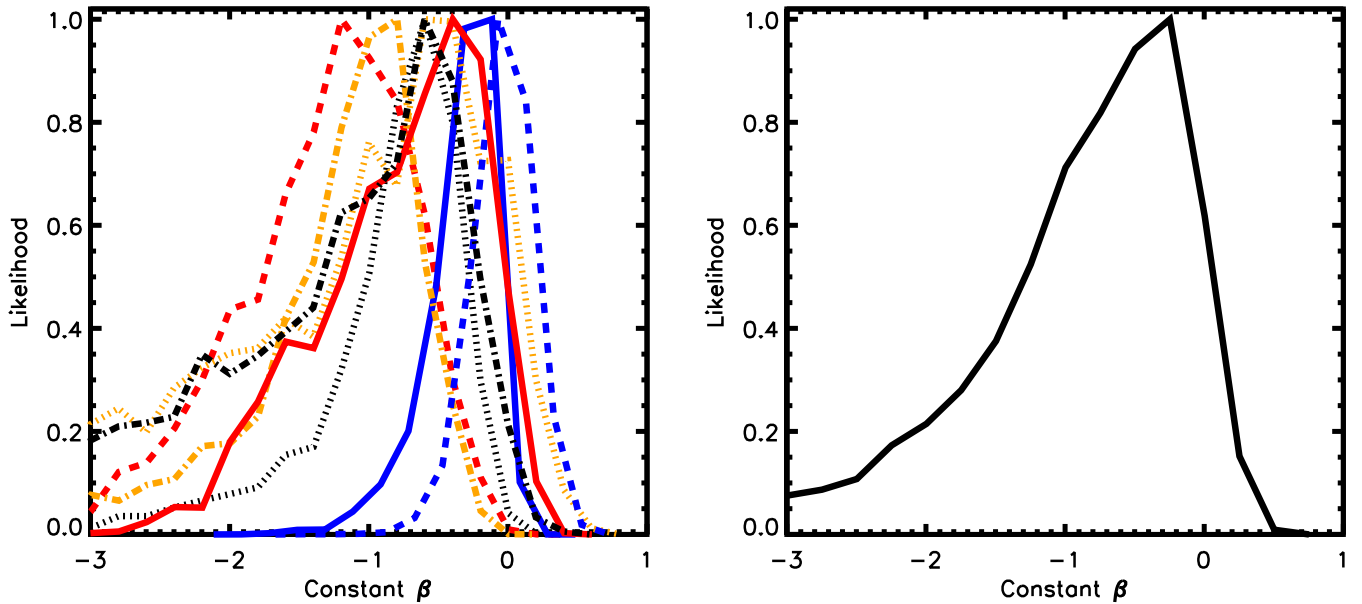


Figure 3. The posterior distribution of anisotropy (assumed to be spatially constant) for all of the MW dSphs considered in this paper when the density profile is fixed to be a NFW. The identification scheme is as follows – Carina: black dotted; Draco: red dashed; Fornax: blue solid; Leo I: orange dash dotted; Leo II: orange dotted; Sculptor: blue dashed; Sextans: red solid; and Ursa Minor: black dash dotted. The plot on the right shows that combined likelihood for β when each dSph is given equal weight. It is clear that the data demand a tangential anisotropy in the velocity dispersion tensor for cuspy profile fits.

cut in metallicity (which tends to have a broad distribution in dSphs) and the radial density profile for each population is assumed to follow the radial distribution of the red and blue horizontal branch stars obtained through photometry. Uncertainties in this assignment translate to uncertainties in the estimated velocity dispersion profiles, especially that of the colder population. In addition, the radial distribution of the tracer populations should reflect these uncertainties (and they should not be completely fixed from fits to the photometric sample). Freedom in the radial distribution of the subpopulations would imply (as the analytic results of W10 show) that the locations where the mass is well-constrained become more uncertain, thus making estimates of the mass profile and its derivative dependent on assumptions regarding the stellar velocity anisotropy.

A related issue concerns foreground subtraction that may have benign effects for the entire population as a whole, but could affect one population more significantly than another. Further complications arise when one of the populations is much more centrally concentrated, as is the case for the metal rich population identified in B08. The isophotal ellipticities could be different in the inner parts (for Sculptor, see Demers et al. 1980) and adopting a half-light radius for each population without accounting for these effects could lead to a bias. A detailed investigation of these issues, following the seminal work of B08, is required but it is beyond the scope of this paper.

3.5 Stellar velocity dispersion anisotropy in a Λ CDM context

Dissipationless Λ CDM simulations predict that dark matter halos generally follow cuspy density profile distributions over observable scales. For concreteness, we force the dynamical

mass to be a NFW profile ($a = 1$, $b = 3$, $c = 1$ in Equation 4) and then derive the posterior distributions of β implied by the kinematic data. Our aim is to gain some insight on values of anisotropy required of these dSphs should they be embedded in a cuspy halo.

Our results can be seen in Figure 3, where on the left-hand plot we superimpose the β distributions of all eight dSphs. The right-hand plot shows the combined likelihood of all weighted equally. For most of the dSphs, tangentially anisotropic velocity dispersions are favored. The 68% range for the combined sample is $-1 \leq \beta \leq 0$. We note that this range is lower than what is generally reported for the anisotropy of dark matter particles, which typically are close to isotropic in the central regions and become radially anisotropic in the outer parts of the halo. However, there is no theoretical reason to expect the anisotropy of stars to be the same as that of dark matter.

It is important to recognize that Λ CDM simulations predict not just the radial density profile of dark matter, but also the range of scale radii expected for a given subhalo mass or V_{\max} (i.e. the subhalo concentration). This amounts to a prediction for the log slope as a function of physical radius. In Figure 3 we fixed the density profiles to be NFW but we did not force the scale radii to match those of subhalos predicted in Λ CDM simulations. Now we aim to investigate whether the derived $\gamma(r_{1/2})$ values are consistent with subhalos of the appropriate concentration for their mass scale from high-resolution dissipationless Λ CDM simulations.

The solid lines in each panel of Figure 4 show the predicted log-slope run for a $V_{\max} = 17$ km/s Einasto profile halo with a scale radius set by the median of the Aquarius simulation. Note that, even though it is not shown, this halo has the appropriate density normalization to provide a good match to the points in the left panel of Figure 2. It should be

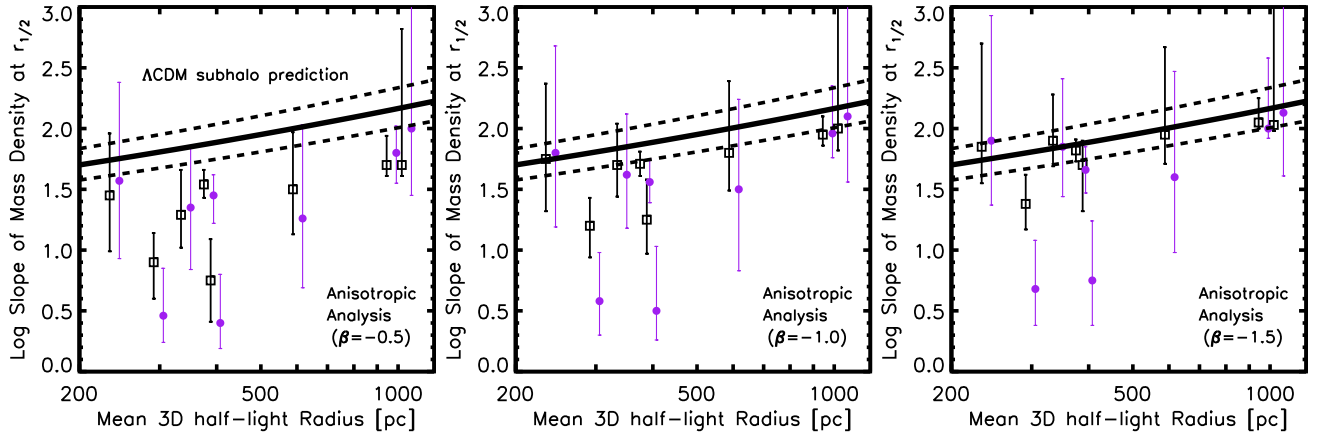


Figure 4. Squares show our derived log-slope of the mass density at the deprojected half-light radius for each dSph assuming the general density profile in Equation 4. As marked, each panel presents a different choice of (tangentially biased) velocity dispersion anisotropy β . The solid black line, which is the same in each panel, shows the median expectation for $V_{\max} = 17$ km/s subhalos in the Aquarius simulation. The dashed lines show the one-sigma deviation from this relation. We see that in order for the MW dSphs to be consistent with the expectations for dissipationless Λ CDM subhalos, the stars must have a substantially larger tangential velocity dispersion than radial velocity dispersion. The purple circles, arbitrarily offset to the right for clarity, show a test that explores the sensitivity of our results to uncertainties in the central light profile. For these points, we have removed data for on-sky radii $R < r_{1/2}$ and we recomputed the log-slopes. We see that the overall result is insensitive to the inner data.

noted that the radial dependence on the predicted log-slope from Λ CDM simulations does not change dramatically for subhalos that span reasonable V_{\max} ranges.

The black open squares in the three panels of Figure 4 show our derived results for $\gamma(r_{1/2})$ for three choices of anisotropy ($\beta = -0.5, -1.0$ and -1.5). In deriving these points we have allowed a fully general halo profile (restoring freedom to all of the variables in Equation 4). As one moves from left to right in the panels, one can see that the only way for the dSphs to be consistent with the median subhalo expectation is for the velocity dispersion tensor of the stars to be tangentially anisotropic ($\beta \simeq -1.5$).

One concern with this result is that uncertainties in the stellar density profile shape will hinder our ability to accurately derive $\gamma(r_{1/2})$. The purple circles in Figure 4 (offset arbitrarily to the right for clarity) show results of a test designed to explore this possibility. Here we have removed data in the on-sky region $R < \frac{1}{2}r_{1/2}$. We found that our results for $\gamma(r_{1/2})$ did not vary much (i.e. compare the purple circles to the black squares, which were calculated with all of the data). This implies that the slope of the density profile at the deprojected half-light radius is determined predominantly by the local velocity measurements, and thus the uncertainty of the inner light profile does not contribute significantly to the derived values of $\gamma(r_{1/2})$ for the MW dSphs we are investigating.

The main point to take from this subsection is that in order to decently model the classical MW dSphs as galaxies living embedded inside of subhalos in Λ CDM-based simulations (or even arbitrary NFW halos), a negative β for the stars is usually required. By imposing $\beta = 0$ in the first half of this paper, we have been stacking the odds against finding cuspy halos. By simply adjusting all of the anisotropies to mildly negative values most of the dSphs can live in cuspy halos. Nevertheless, unless the negative anisotropy is significant, those cuspy halos are typically *less concentrated* than expected for subhalos of the appropriate mass. In order to

achieve an overall match to subhalo scaling relations, fairly significant tangential anisotropies are required ($\beta \simeq -1.5$).

4 CONCLUSIONS

We have performed dynamical Jeans analyses on the eight classical Milky Way dwarf spheroidal galaxies and we have explored their central density structure in comparison to predictions for subhalos in dissipationless Λ CDM simulations. We find that in the limiting case of an isotropic velocity dispersion ($\beta = 0$), the classical MW dSphs predominantly prefer to live in halos that are less concentrated than predicted in these simulations. In order to achieve an overall match to the cuspy profile shapes and subhalo concentrations expected from dissipationless Λ CDM simulations, fairly significant tangential velocity dispersion anisotropy is required ($\beta \simeq -1.5$). This result is reminiscent of the well-known central density problem faced by Λ CDM (e.g. Alam et al. 2002) in comparison to higher mass galaxies. This effect is also perhaps related to the findings of Boylan-Kolchin et al. (2011, 2012), who find that the classical MW dSphs are not dense enough to host the expected number of massive subhalos around Milky Way size galaxies. The unexpectedly low concentrations of the dwarf spheroidal galaxies might be explained by stochastic feedback effects, which in principle lower the densities of dark matter halos compared to what is predicted in dissipationless simulations (e.g. Mashchenko et al. 2008; Brook et al. 2011; Governato et al. 2010; Pasetto et al. 2010; Oh et al. 2011). Another possibility is that the dark matter itself is non-standard (e.g. Vogelsberger et al. 2021).

Solutions to the isotropic Jeans equation show that not all of the MW dSphs prefer to live in halos that have constant density cores at small radii, even with a conservative treatment of the stellar density profile. As summarized in Table 1 and Figure 1, four of the eight dSphs are consistent

with $\gamma = 1$ central cusps at one sigma. Sculptor strongly favors a cuspy inner profile ($\gamma \simeq 1$), while Fornax and Sextans prefer mild cusps ($\gamma \simeq 0.7$), albeit with large uncertainties. Three galaxies (Carina, Draco, and Leo I) demonstrate a preference for a core ($\gamma \simeq 0$). Therefore, our work lays to rest the possibility that the assumptions of isotropy and equilibrium force the inner density profiles of all of the MW dSphs to be cored. Rather, we have shown that the assumption of isotropy demands that their *concentrations* are lower than predicted in Λ CDM, regardless of the presence of a true core in the profile.

Relaxing either the isotropy constraint or the shape of the inner stellar density profile broadens the allowed range of inner density slopes. If we adjust all of the anisotropies to negative values most of the dSphs prefer to live in cuspy halos.

We also explored whether it was possible to find a common cored dark matter halo that simultaneously fits the average local density at $r_{1/2}$ and the local log-slope at $r_{1/2}$ under the assumption of isotropy. We showed that such a common halo is not possible when restricted to the family of Burkert profiles advocated by D09, but that the NFW profile used by W10 is a more reasonable fit. If we drop the log-slope constraint derived assuming isotropy, then we can find a single Burkert profile which matches the density-radius relation for the classical MW dSphs, as long as the core radius is smaller than the typical size of any galaxy in the population ($r_{\text{core}} \lesssim 200$ pc). Interestingly, one of the common Burkert halos with which we fit the local density at $r_{1/2}$ is actually steeper than the W10 NFW halo over the radii probed by the data.

Acknowledgements – We would like to thank Manoj Kaplinghat, Greg Martinez, and Louie Strigari for helpful discussions and we acknowledge partial support from NASA grant NNX09AD09G.

REFERENCES

- Alam, S. M. K., Bullock, J. S., & Weinberg, D. H. 2002, *ApJ*, 572, 34
- Amorisco, N. C. & Evans, N. W. 2012, *MNRAS*, 419, 184
- An, J. H. & Evans, N. W. 2006, *ApJ*, 642, 752
- Avila-Reese, V., Colín, P., Valenzuela, O., D’Onghia, E., & Firmani, C. 2001, *ApJ*, 559, 516
- Battaglia, G., Helmi, A., Tolstoy, E., Irwin, M., Hill, V., Jablonka, P. 2008, *ApJ*, 681, 13
- Boylan-Kolchin, M., Bullock, J. S., & Kaplinghat, M. 2011, *MNRAS*, L267
- Boylan-Kolchin, M., Bullock, J. S., & Kaplinghat, M. 2012, *arXiv:1111.2048*
- Burkert, A., 1995, *ApJ*, 447L, 25
- Brook, C. B., et al. 2011, *MNRAS*, 415, 1051
- de Blok, W. J. G., McGaugh, S. S., Rubin, V. C. 2001, *AJ*, 122, 2396
- de Blok, W. J. G. 2010, *Advances Astron.*, 2010, 5
- de Bruijne, J. H. J., van der Marel, R. P., & de Zeeuw, P. T. 1996, *MNRAS*, 282, 909
- Demers, S., Krautter, A., & Kunkel, W. E. 1980, *AJ*, 85, 1587
- Diemand, J., Kuhlen, M., Madau, P., Zemp, M., Moore, B., Potter, D., Stadel, J. 2008, *Nature*, 454, 735
- Donato, F. et al. 2009, *MNRAS*, 397, 1169
- Dubinski, J., & Carlberg, R. G. 1991, *ApJ*, 378, 496
- Einasto, J. 1965, *Trudy Inst. Astrofiz. Alma-Ata*, 51, 87
- Flores, R. A. & Primack, J. R. 1994, *ApJ*, 427, 1
- Geha, M., Willman, B., Simon, J. D., Strigari, L. E., Kirby, E. N., Law, D. R., Strader, J. 2009, *ApJ*, 692, 1464
- Gilmore, G., Wilkinson, M. I., Wyse, R. F. G., Kleyana, J. T., Koch, A., Evans, N. W., Grebel, E. K. 2007, *ApJ*, 663, 948
- Governato, F., et al. 2010, *Nature*, 463, 203
- Hogan, C. J., & Dalcanton, J. J. 2000, *Phys Rev D*, 62, 063511
- Hernquist, L. 1990, *ApJ*, 356, 359
- Kalirai, J. S., Beaton, R. L., Geha, M. C., Gilbert, K. M., Guhathakurta, P., Kirby, E. N., Majewski, S. R., Osthheimer, J. C., Patterson, R. J., Wolf, J. 2010, *ApJ*, 711, 671
- Kaplinghat, M. 2005, *Phys Rev D*, 72, 063510
- King, I. 1962, *AJ*, 67, 471
- Klypin, A., Kravtsov, A. V., Valenzuela, O., Prada, F. 1999, *ApJ*, 522, 82
- Koch, A., Kleyana, J. T., Wilkinson, M. I., Grebel, E. K., Gilmore, G. F., Evans, N. W., Wyse, R. F. G., Harbeck, D. R. 2007, *AJ*, 134, 566
- Komatsu, E. et al. 2011, *ApJS*, 192, 18
- Kuzio de Naray, R., McGaugh, S. S., de Blok, W. J. G. 2008, *ApJ*, 676, 920
- Kuzio de Naray, R., Martinez, G. D., Bullock, J. S., & Kaplinghat, M. 2010, *ApJL*, 710, L161
- Lokas, E. L. 2009, *MNRAS*, 394, 102
- Mamon, G. A. & Boué, G. 2010, *MNRAS*, 401, 2433
- Martinez, G. D., Bullock, J. S., Kaplinghat, M., Strigari, L. E., Trotta, R. 2009, *JCAP*, 06, 014
- Martinez, G. D., Minor, Q. E., Bullock, J., Kaplinghat, M., Simon, J. D., Geha, M. 2011, *ApJ*, 738, 55
- Mashchenko, S., Wadsley, J., Couchman, H. M. P. 2008, *Science*, 319, 174
- Mateo, M., Olszewski, E. W., Pryor, C., Welch, D. L., Fischer, P. 1993, *AJ*, 105, 510
- Mateo, M., Olszewski, E. W., Walker, M. G. 2008, *ApJ*, 675, 201
- Moore, B. 1994, *Nature*, 370, 629
- Moore, B., Ghigna, S., Governato, F., Lake, G., Quinn, T., Stadel, J., Tozzi, P. 1999, *ApJ*, 524, L19
- Muñoz, R. R. et al. 2005, *ApJ*, 631, 137
- Navarro, J. F., Frenk, C. S., White, S. D. M. 1997, *ApJ*, 490, 493
- Oh, S.-H., Brook, C., Governato, F., Brinks, E., Mayer, L., de Blok, W. J. G., Brooks, A., Walter, F. 2011, *AJ*, 142, 240
- Pasetto, S., Grebel, E. K., Berczik, P., Spurzem, R., Dehnen, W. 2010, *A&A*, 514A, 47
- Peñarrubia, J., Benson, A. J., Walker, M. G., Gilmore, G., McConnachie, A. W., Mayer, L. 2010, *MNRAS*, 826
- Plummer, H. C. 1911, *MNRAS*, 71, 460
- Simon, J. D., Bolatto, A. D., Leroy, A., Blitz, L. 2003, *ApJ*, 596, 597
- Simon, J. D., Bolatto, A. D., Leroy, A., Blitz, L., Gates, E. L. 2005, *ApJ*, 621, 757
- Simon, J. D. & Geha, M. 2007, *ApJ*, 670, 313

- Simon, J. D., et al. 2011, *ApJ*, 733, 46
- Springel, V. et al. 2008, *MNRAS*, 391, 1685
- Strigari, L. E., Bullock, J. S., Kaplinghat, M. 2007a, *ApJ*, 657L, 1
- Strigari, L. E., Bullock, J. S., Kaplinghat, M., Diemand, J., Kuhlen, M., Madau, P. 2007b, *ApJ*, 669, 676
- Strigari, L. E., Kaplinghat, M., & Bullock, J. S. 2007c, *Phys Rev. D*, 75, 061303
- Strigari, L. E., Bullock, J. S., Kaplinghat, M., Simon, J. D., Geha, M., Willman, B., Walker, M. G. 2008, *Nature*, 454, 1096
- Strigari, L. E., Frenk, C. S., White, S. D. M. 2010, *MNRAS*, 408, 2364
- Tollerud, E. J., Bullock, J. S., Graves, G. J., Wolf, J. 2011, *ApJ*, 726, 108
- Vogelsberger, M., Zavala, J., Loeb, A. 2012, *arXiv:1201.5892*
- White, S. D. M. 1981, *MNRAS*, 195, 1037
- Walker, M. G., Mateo, M., Olszewski, E. W., Gnedin, O. Y., Wang, X., Sen, B., Woodroffe, M. 2007, *ApJ*, 667, 53
- Walker, M. G., Mateo, M., Olszewski, E. W. 2009a, *AJ*, 137, 3100
- Walker, M. G., Mateo, M., Olszewski, E. W., Peñarrubia, J., Wyn Evans, N., Gilmore, G. 2009b, *ApJ*, 704, 1274
- Walker, M. G., Mateo, M., Olszewski, E. W., Sen, B., & Woodroffe, M. 2009, *AJ*, 137, 3109
- Walker, M. G. and McGaugh, S. S. and Mateo, M. and Olszewski, E. W. and Kuzio de Naray, R. 2010, *ApJ*, 717, 87
- Willman, B. 2010, *Advances Astron.*, 2010, 285454
- Willman, B., Geha, M., Strader, J., Strigari, L. E., Simon, J. D., Kirby, E., Warres, A. 2011, *AJ*, 142, 128
- Wolf, J., Martinez, G. D., Bullock, J. S., Kaplinghat, M., Geha, M., Muñoz, R. R., Simon, J. D., Avedo, F. F. 2010, *MNRAS*, 406, 1220